Hindawi
Advances in Materials Science and Engineering
Volume 2023, Article ID 6232579, 8 pages
https://doi.org/10.1155/2023/6232579

Research Article

Mechanism of Imprinting Process in the Ni-P Metallic Glass Films: A Molecular Dynamics Study

Tri Widodo Besar Riyadi,[1] Ramaswamy Sivaraman,[2] Alaa Mohammed Hussein Wais,[3] Farag M. A. Altalbawy,[4,5] Ulugbek Oybutaevich Khudanov,[6] and Dinesh Kumar Chaudhary[7]

[1]*Faculty of Engineering, Universitas Muhammadiyah Surakarta, Surakarta, Indonesia*
[2]*Department of Mathematics, Dwaraka Doss Goverdhan Doss Vaishnav College, University of Madras, Chennai Arumbakkam, India*
[3]*Biomedical Engineering Department, Al-Mustaqbal University College, Hillah 51001, Babil, Iraq*
[4]*National Institute of Laser Enhanced Sciences (NILES), Cairo University, Giza 12613, Egypt*
[5]*Department of Chemistry, University College of Duba, Tabuk University, Duba 71911, Saudi Arabia*
[6]*Department of Chemistry and Its Teaching Methods, Jizzakh State Pedagogical Institute Named After Abdullah Kadiri, Jizzakh, Uzbekistan*
[7]*Department of Physics, Amrit Campus, Tribhuvan University, Kathmandu, Nepal*

Correspondence should be addressed to Dinesh Kumar Chaudhary; din.2033@gmail.com

Received 28 July 2022; Revised 18 October 2022; Accepted 18 January 2023; Published 31 January 2023

Academic Editor: Shahin Khademinia

In this study, the molecular dynamics (MD) simulation was used to evaluate the role of imprinting temperature and the mold-cavity geometry on the imprinted Ni-P metallic glass (MG) films. Considering the outcomes of simulation, it was found that the tip-like and groove patterns showed different filling time for the imprinting process. At room temperature (300 K), the plastic deformation in the tip-like pattern was in a ring shape enclosing the mold, while the plastic deformation in the groove-pattern geometry was mainly localized at the wall of mold. Moreover, it was determined that the imprinting at high temperature (700 K) led to the shortening of pattern filling time and the decrease of loading force in both geometries. The strain concentration and localized plastic deformation were also removed in the high-temperature imprinting process. On the other hand, the unloading process at room temperature (300 K) improved the imprinting quality due to the lower elastic recovery.

1. Introduction

Fabrication of engineering components at micro/nanoscale is one of the huge challenges in the high-tech industries [1–3]. To overcome this issue, nanoimprinting lithography (NIL) has been proposed as a novel technique in which the fabricated patterns and components are the potential candidates for application in optical devices, micro-integration systems, nanomold production, and biological devices [4, 5]. In this method, a mechanical deformation process is conducted to transfer the pattern onto the metallic films by an imprinting-release procedure [6–8].

Due to their disordered atomic structure, metallic glasses (MGs) typically exhibit superior mechanical properties and excellent viscous flow formability [9–13]. Hence, a great interest has been taken by researchers to employ this kind of metallic alloys in the NIL method [14–16]. To provide sample examples, Xiaoyu et al. [17] indicated that the $Fe_{40}Co_{35}P_{10}C_{10}B_5$ amorphous alloy is a favored composition for producing various nano-patterns with adaptable magnetic properties. Li et al. [18] fabricated a nano-patterned template with an amorphous surface through the electrodeposition technique. Their results indicated that the nanoimprint templates exhibited an excellent flexibility and

environmental stability, which was suitable for high-resolution imprint lithography with good industrialization prospects. Using molecular dynamics (MD) simulation, the pattern transfer mechanism of ZrCu MG films under a nanoimprinting process was evaluated, and it was found that the imprinting at large aspect ratio or high temperatures shortened the filling time [19]. Doan et al. [20] indicated that the increase in angle of the punch led to rise of imprinting force and the shear transformation zones (STZs) of the CuZr glassy films. Wu and Hou [21] unveiled that the imprinting process was more efficient at the temperature slightly higher than the glass transition temperature, followed by unloading at room temperature. It was also determined that the tip-like pattern on the mold required a smaller loading force and longer filling time, compared to the groove pattern. Another investigation exhibited that the capillary force and boundary condition played crucial roles in the nanoimprinting process, and the mold filling speed was influenced by the thickness of MG films [22]. Singer et al. [23] applied sacrificial imprint lithography for multiscale patterning of MGs, in which the cost and complexity of generating controlled nanostructures on sophisticated geometries were eliminated. Wang et al. [24] produced large dimensions of nanostructures using an inexpensive thermal imprint method in air with a new composition of Au-based MG exhibiting negative dielectric constants. The $Cu_{50}Zr_{25}Ti_{25}$ MG was also selected for the NIL patterning, and the corresponding microstructural investigations showed that the STZs were generated at the substrate surface underneath the mold during the forming process [25]. Tran et al. [26] investigated the NIL process of CuAgAu films through MD simulation and found that the change in the change in imprinting conditions markedly affected the final mechanical properties and induced the nanocrystallization in the structure. Wang et al. [27] reported that the deformation mechanism of Ni-Zr glassy film can be described through the rearrangement of short-range scale clusters with fractal configuration. It was also demonstrated that the pileup index strongly depended on the temperature and alloying composition in the Ni-Zr amorphous films. Kumar et al. [28] developed a model based on the flow and pressure fields in the NIL process of MGs. They also took into account an additional threshold pressure for breaking the oxide layer on the MG surfaces.

As depicted, the NIL process of MGs plays a crucial role in the production of microcomponents. Hence, it is important to characterize the mechanism of plastic deformation and the mechanics of imprinting for obtaining the optimal parameters. This work aims to analyze the atomic-scale features of imprinted MG films through the MD simulation. Using the atomic-scale modeling, it is possible to accurately study the thermodynamics and mechanical properties by preventing the experimental noises [29–31].

2. Computational Methodology

For MD simulation, the $Ni_{80}P_{20}$ MG was constructed through the embedded-atom method (EAM) potential of the Ni-P system proposed by Sheng et al. [32]. To establish the atomic configuration, the Ni and P atoms with a random distribution were heated to the temperature of 2100 K and kept for 2 ns. Afterwards, the melted alloy was quenched to the room temperature with cooling rate of 10^{11} K/s, followed by a relaxation treatment at 500 K to remove any cooling effect. This simulation was carried out under the isothermal isobaric ensemble (NPT) and time step of 1 fs through the large-scale atomic/molecular massively parallel simulator code. Moreover, the three-dimensional periodic boundary conditions (PBCs) were considered for the simulation and the temperature was controlled by the Nosé–Hoover thermostat [33].

Figure 1 shows that the NIL physical model includes a rigid mold along with the Ni-P MG film, which was cut from the atomic block prepared previously. The NIL process was carried out with two types of patterns, facilitating the evaluation of mold-cavity geometry effects. The MG films included two types of atoms, i.e., Newtonian atoms and fixed atoms, in the simulation. The fixed atoms, located at the top of film, stabilized the whole system during the NIL process. Furthermore, the NVT ensemble and PBCs (at X and Y directions) were applied in the simulation. In the NIL process, the imprinting was conducted through the constant movement of mold (5×10^{-5} nm per time step) followed by a holding time of 60 ps at the maximum displacement and finally the mold was unloaded instantly. The details for the evaluation of atomic interaction in the film and mold/film are given in Ref. [21].

3. Results and Discussion

Figure 2 represents the imprinting process by the tip-like mold at the different displacements (D) and constant temperature of 300 K. When the mold touched the MG film at $D = 0$ nm, some of the MG atoms at the surface were adsorbed onto the mold, which was due to the Van der Waals force at the interface. At the initial stage of NIL process ($D = 1.8$ nm), the shear strain gradually increased underneath the mold and it instantly continued with a rise of D value to 2.4 nm. With the further increment of displacement ($D = 3.1$ nm), the high-strained atoms were nucleated from the sides of mold and generated in a ring-like shape in the microstructure of the MG film. These atoms (red regions) are indicative of shear transformation zones (STZs), which are the sources of plastic deformation in the amorphous structure [34]. Finally, one can see that an apparent ring of strained atoms is formed at the D value of 4.5 nm. Unlike mechanism of dislocations in crystalline alloys, the plastic deformation of MGs is defined by the formation and percolation of nanoscale defects such as STZs [35].

The effects of imprinting temperature on the strain distribution of MG films are illustrated in Figure 3. The strain snapshots give the instant of entire tip-like mold filling in the NIL process. As can be seen, the D value for the entire filling significantly decreases with the rise of temperature, which may be owing to the easier cooperative atomic movement at high temperatures. Moreover, it is observed that the higher temperature facilitates the generation of atomic strain in the bulk of film so that the ring-like shape of

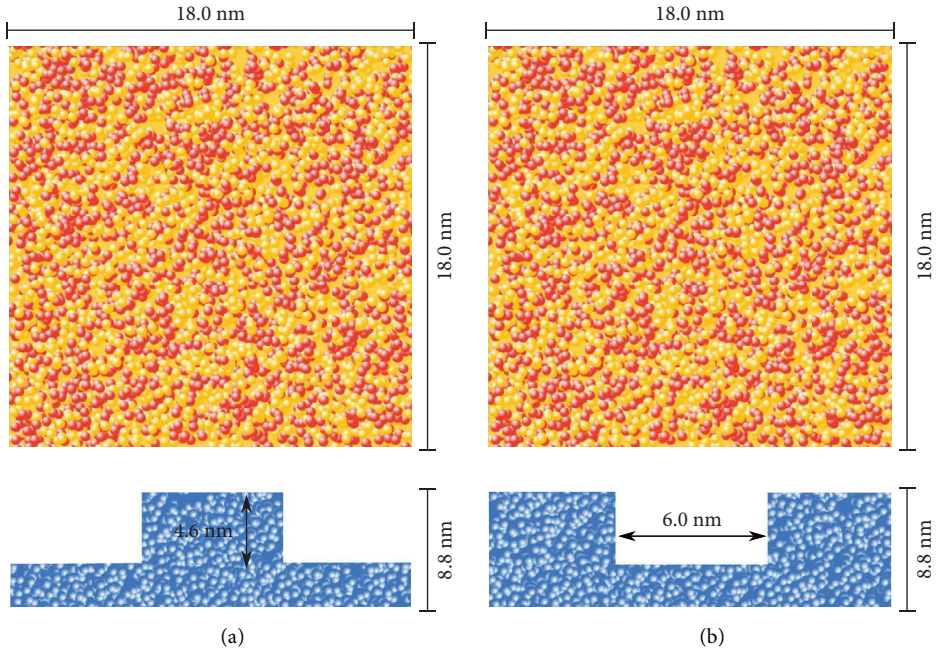

Figure 1: Schematic of (a) tip-like and (b) groove patterns on mold for nanoimprinting process.

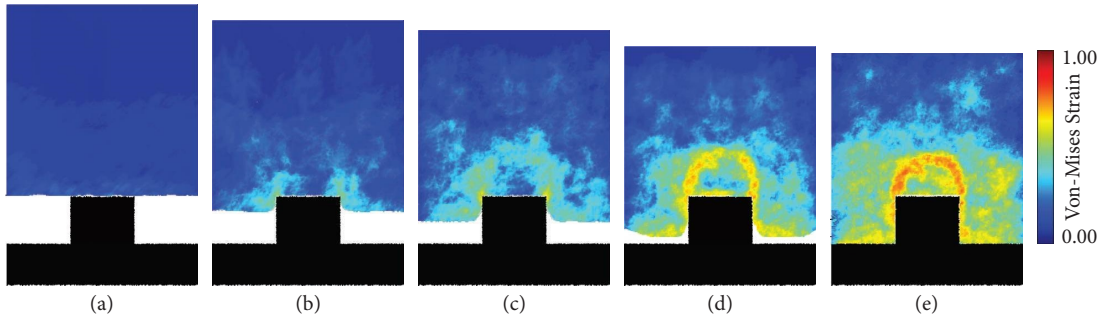

Figure 2: Evolution of imprinting process with tip-like pattern at 300 K for mold displacement of (a) 0 nm, (b) 1.8 nm, (c) 2.4 nm, (d) 3.1 nm, and (e) 4.5 nm.

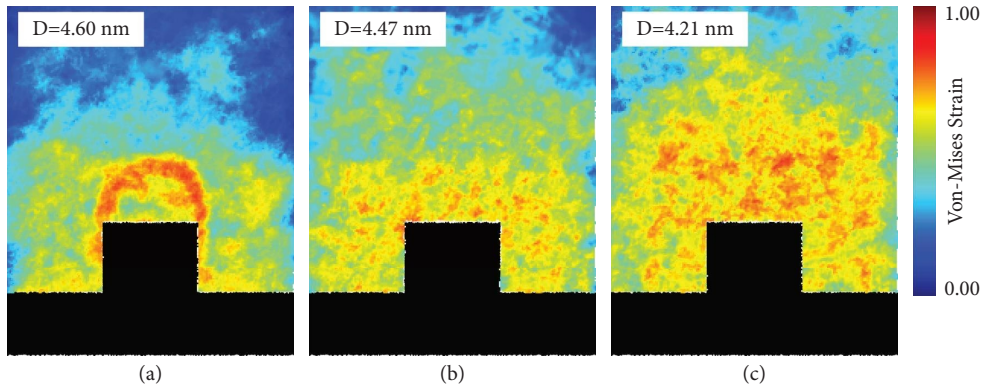

Figure 3: Imprinting process with tip-like pattern in the complete filling stage at (a) 300 K, (b) 500 K, and (c) 700 K.

induced strain at 300 K approximately disappears in the sample imprinted at 700 K (above the glass transition temperature). Figure 4 shows the loading force and filling height as a function of mold displacement for imprinting process at 300 K, 500 K, and 700 K. At the beginning of NIL process, the curves show a negative value which is related to

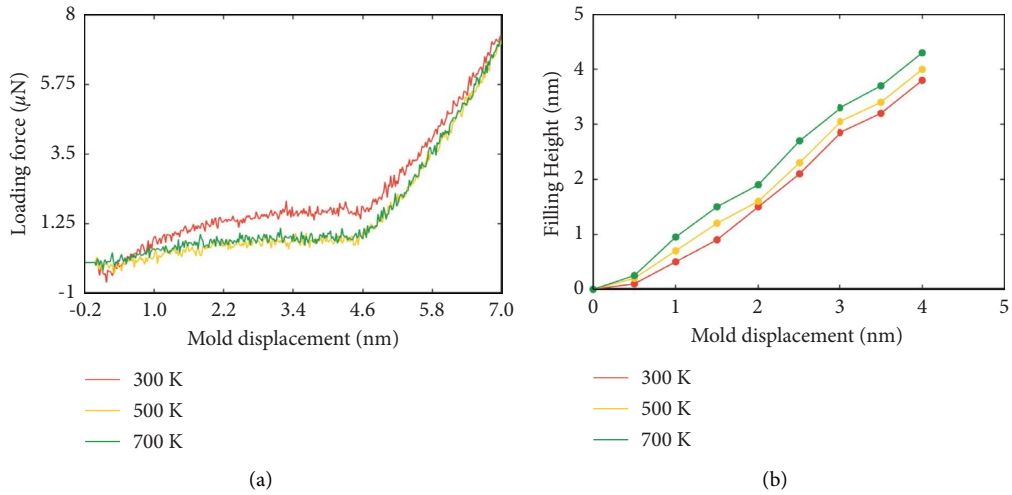

Figure 4: (a) Loading force and (b) filling height as a function of mold displacement for the tip-like pattern imprinting process.

the Van der Waals attractive force between the MG film and the mold (see Figure 4(a)). This negative force is more intensified at lower temperatures. With the increase of mold displacement, the loading force gently rises so that a steady state can be detected in the middle of the imprinting process. Finally, a sharp increment of loading occurs, which is due to the overfilling. In all the imprinting temperatures, the trend of loading force is similar; however, it is clearly found that the lower temperature (300 K) intensifies the force variations. This is due to the fact that the energy barrier for atomic rearrangement and STZ formation is higher at room temperature [21, 22]. Figure 4(b) shows that the high temperature improves the filling efficiency so that the amorphous film readily flows into the cavity and completes the imprinting process at shorter times.

It is feasible to study the recovery of elastic features in the imprinted samples after the unloading. As can be seen in Figure 5(a), there are geometrical parameters defining the elastic recovery in the system. In this criterion, W, H, and h are width of the pattern, height of the whole film, and height of the whole film minus the height of the pattern, respectively. Moreover, W', H', and h' are the indicative of geometrical dimensions after the elastic recovery. Using the mentioned parameters, the elastic recovery can be defined as follows [21]:

$$\eta_{x=(|x-x'|/x)}, \quad (1)$$

in which x and x' are the geometrical parameters before and after the elastic recovery, respectively. Figure 5(b) depicts the change of elastic recovery ratios as a function of imprinting temperature for the tip-like mode. It is found that the mean lowest recovery of elasticity occurs at the room temperature (300 K), meaning that the low-temperature unloading does not significantly affect the final geometry of the imprinted sample. With the rise of temperature, the elastic recovery is intensified, especially at the width direction. According to the results, the mean elastic recovery in the sample imprinted at 700 K is 3-4 times higher than that in the sample proceeded at the room temperature, indicating that the high temperature may lead to the poor pattern transfer with inaccurate final dimensions.

Figure 6 represents the imprinting process at the different displacements (D) and constant temperature of 300 K through the groove pattern on the mold. As can be seen, the typical extrusion process is similar to the backward NIL process with a groove pattern [21]. At the beginning of the imprinting process ($D = 1.1$ nm), some part of MG film is extruded into the groove of mold, leading to the formation of a bow at the arrival. With the increase of D value to 2.9 nm, the extruded atoms into the groove part of the mold markedly rise so that the bow is extended in the groove space. As marked in the figure, the angle between the mold wall and the bow is identified as the dynamic contact angle ($\theta \sim 131^{\circ}$). The θ value measured in this work is similar to that reported in other investigations focusing on the MGs and polymers [21, 36]. Finally, the groove is completely filled at $D = 4.3$ nm, in which the localized shear strain occurs at the mold walls and the arrival of the groove. It is suggested that the application of the loading force during the NIL process leads to significant stress concentration at the mold walls and subsequent atomic rearrangements in this region. The effects of imprinting temperature on the strain distribution of MG films extruded in the groove mold are illustrated in Figure 7. Similar to the tip-like pattern on mold, the NIL process at higher temperatures declines the time of filling, which is due to the improvement of plastic deformation. Moreover, one can see that the higher temperature leads to the extension of atomic movement from the mold walls and the bow position to the bulk of groove and some regions underneath the mold. It is believed that the higher temperature decreases the energy barrier for the nanoscale atomic rearrangement, and consequently, the atoms in the bulk of samples can locally move and form new structural configurations. In general, the MGs have amorphous structures, in which the loosely packed regions such as free volumes or STZs are embedded in the glassy matrix with densely packed structures [37, 38]. At the higher temperatures, the generation and percolation of loosely packed regions are facilitated, and as a consequence, the plastic deformation is extended in the bulk of material. However,

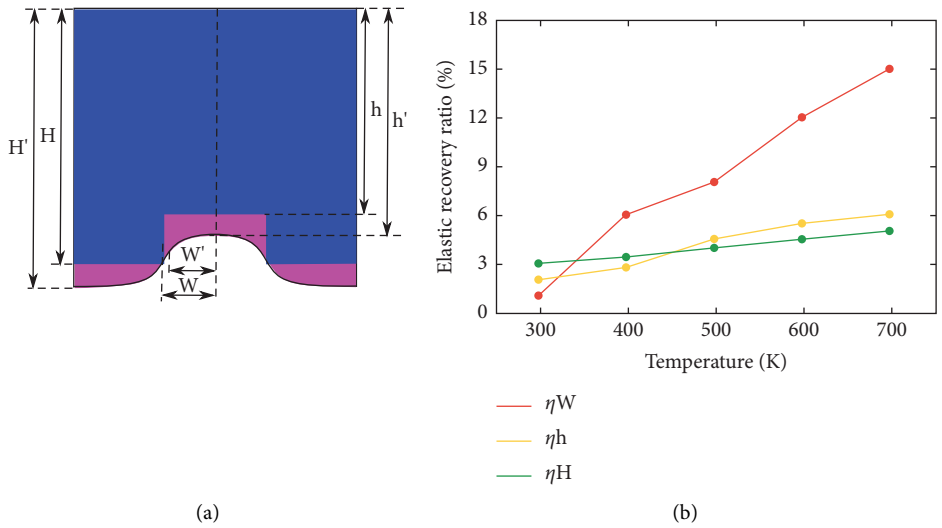

Figure 5: (a) Illustration of parameters defining the elastic recovery and (b) elastic recovery as a function of imprinting temperature for the tip-like pattern.

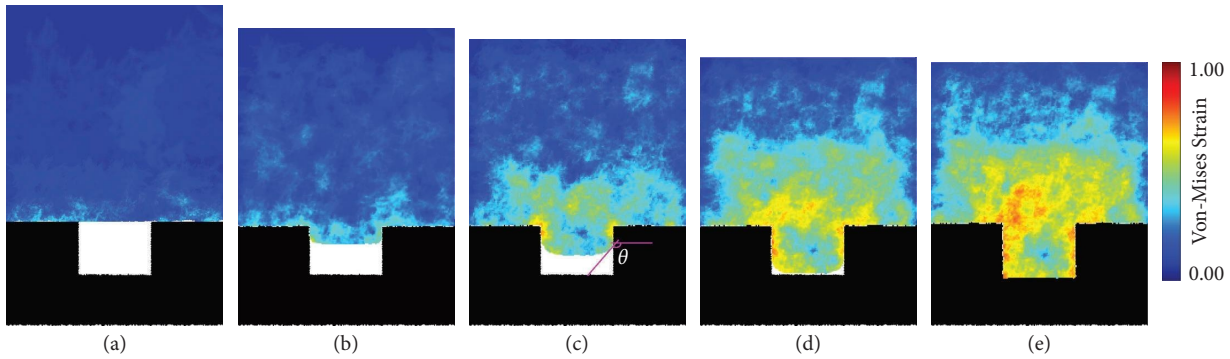

Figure 6: Evolution of imprinting process with groove pattern at 300 K for mold displacement of (a) 0 nm, (b) 1.1 nm, (c) 2.9 nm, (d) 3.5 nm, and (e) 4.38 nm.

one should note that the mentioned event is resulted by the MD simulation, in which the NIL process is conducted in nanoseconds. In the real conditions, the process time is longer which may induce structural relaxation in the MG film so that the imprinting temperature shows a reverse effect. Hence, it is strongly suggested that the high temperature imprinting process for amorphous alloys should be performed in a short time.

Figure 8 indicates the loading force and filling height as a function of mold displacement for the imprinting process with a groove-like mold at 300 K, 500 K, and 700 K. In comparison to the tip-like mode, the Van der Waals force is much higher which may be owing to the larger contact area between the MG film and the mold at the beginning of imprinting process. Furthermore, the fluctuation of loading force, i.e., serrations, is more intensified in this mode, meaning that there is strong interaction between the mold and film. However, Figure 8(b) clearly determines that the groove pattern on the mold improves the performance of filling during the NIL process. This result shows that the mold walls in the groove pattern concentrate the induced stress and enhance the rate of plastic deformation during the process.

As can be observed in Figure 9(a), there also exist geometrical features enabling the evaluation of elastic recovery in the NIL process. In this criterion, W_a' and W_b' are the width of the pattern at the top and the bottom after the recovery, respectively. Moreover, h_1 and h_2 are the height of the whole film and the height of the whole film minus the pattern height, respectively. Using equation (1), it is possible to estimate the elastic recovery based on the mentioned parameters. Figure 9(b) represents the trend of elastic recovery as a function of imprinting temperature for the groove-pattern mold. Similar to the tip-like pattern, the low-temperature process at 300 K leads to the minimum recovery, while the rise of temperature can increase the average elastic variations more than 6-7 times. It is also detected that the increment of pattern width at the top is markedly higher than that at the bottom, implying huge expansion at the width direction. In summary, it was concluded that the high temperature is suitable for the loading stage, while the room temperature should be considered for the unloading stage to minimize the elastic recovery in the imprinted film.

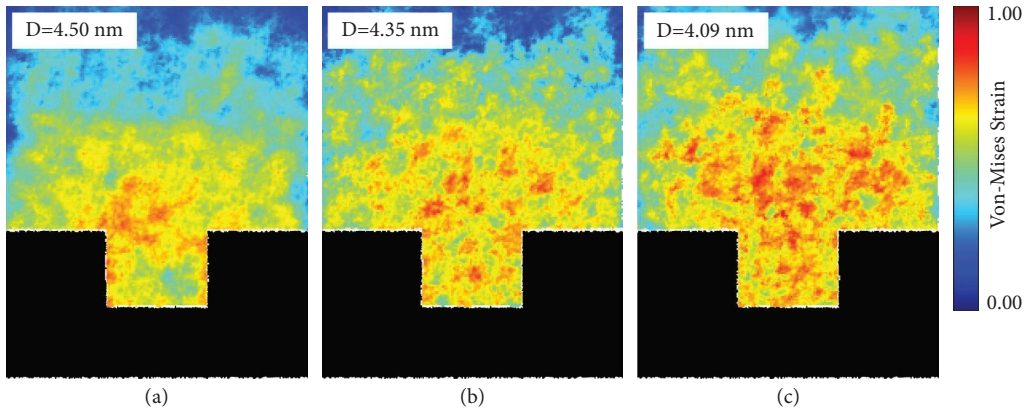

Figure 7: Imprinting process with groove pattern in the complete filling stage at (a) 300 K, (b) 500 K, and (c) 700 K.

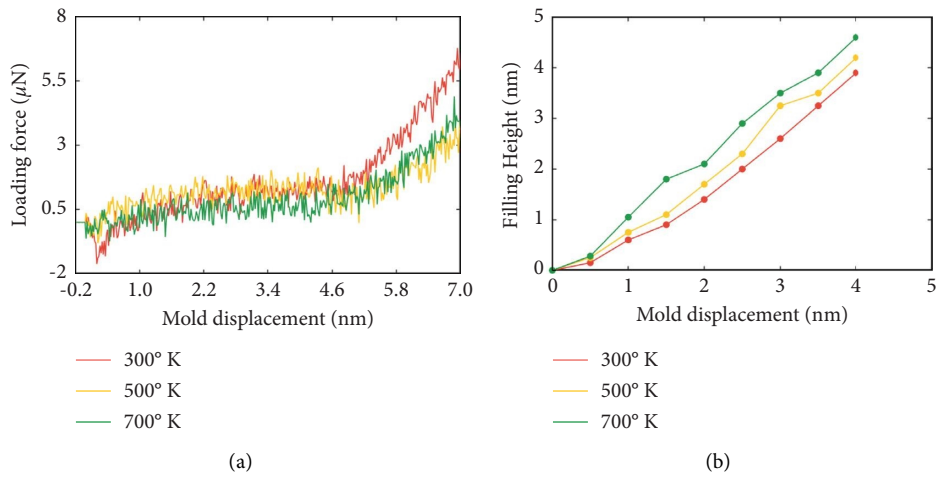

Figure 8: (a) Loading force and (b) filling height as a function of mold displacement for the groove pattern imprinting process.

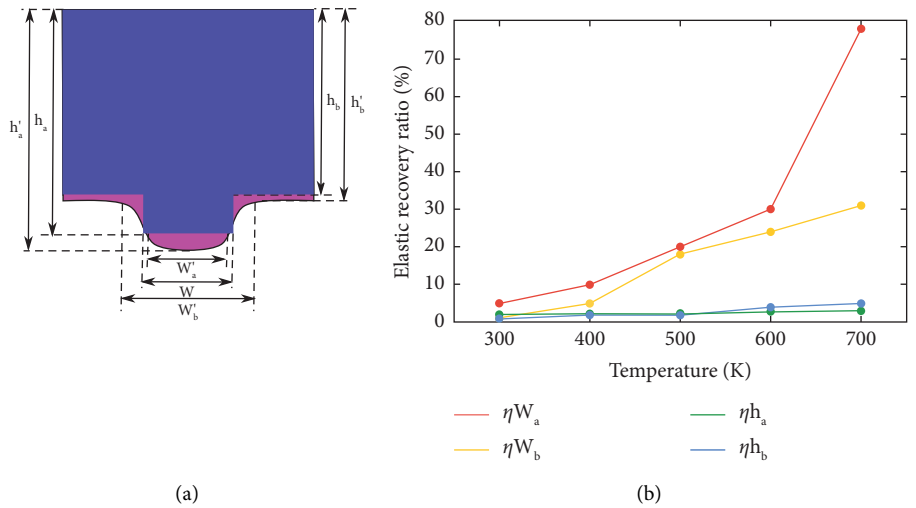

Figure 9: (a) Illustration of parameters defining the elastic recovery and (b) elastic recovery as a function of imprinting temperature for the groove pattern.

4. Conclusion

In this study, the MD simulation was applied to show the influence of imprinting temperature and mold geometry on the quality of imprinted MG films. Based on the MD outcomes, the tip-like geometry of mold cavity led to the formation of plastic regions in a ring-like shape at 300 K, while the increase in the temperature was the main reason for the distribution STZs in the bulk of the MG structure. On the other hand, the groove pattern intensified the plastic deformation at the mold walls and the entrance of the cavity at 300 K. The plastic deformation was also delocalized in this system at high temperatures. It was also demonstrated that the high imprinting temperature was the major factor declining the essential loading force and shortening the filling time in both of imprinting processes. In both of the imprinting systems, the height direction included the lower elastic recovery than that of the width direction. This event was more apparent in the groove pattern.

Data Availability

The data that support the findings of this study are available from the corresponding author upon reasonable demand.

Conflicts of Interest

The authors declare that they have no conflicts of interest.

References

[1] M. Zhang, C. Han, W. Q. Cao, M. S. Cao, H. J. Yang, and J. Yuan, "A nano-micro engineering nanofiber for electromagnetic absorber, green shielding and sensor," *Nano-Micro Letters*, vol. 13, pp. 27–12, 2021.

[2] T. Zhang, Z. Wen, H. Lei et al., "Surface-microengineering for high-performance triboelectric tactile sensor via dynamically assembled ferrofluid template," *Nano Energy*, vol. 87, Article ID 106215, 2021.

[3] A. Khalid, Y. Wei, M. R. Saleem, and W. A. Lughmani, "Meso scale component manufacturing: a comparative analysis of non-lithography and lithography-based processes," *Journal of Micromechanics and Microengineering*, vol. 32, no. 6, Article ID 63002, 2022.

[4] H. C. Jeong, D. H. Kim, D. W. Lee et al., "Solution-driven imprinting lithography of sol–gel ZnO thin films for liquid crystal display," *Langmuir*, vol. 38, no. 8, pp. 2561–2568, 2022.

[5] B. Liu, Y. Yu, Z. Hu et al., "Ag metal interconnect wires formed by pseudoplastic nanoparticles fluid imprinting lithography with microwave assistant sintering," *Nanotechnology*, vol. 33, no. 27, Article ID 275301, 2022.

[6] B. Kumar, P. S. Choubey, and B. N. S. Bhaktha, "High-quality-factor dye-doped polymeric microdiscs fabricated by soft imprint lithography," *The European Physical Journal - Special Topics*, vol. 231, no. 4, pp. 781–789, 2022.

[7] Y. Lee, H. Chae, K. C. Lee et al., "Fabrication of integrated lensless cameras via UV-imprint lithography," *IEEE Photonics J*, vol. 14, no. 2, pp. 1–8, 2022.

[8] J. H. Kang, K. S. Kim, and K. W. Kim, "Molecular dynamics study on the effects of stamp shape, adhesive energy, and temperature on the nanoimprint lithography process," *Applied Surface Science*, vol. 257, no. 5, pp. 1562–1572, 2010.

[9] J. Wegner, M. Frey, M. Piechotta et al., "Influence of powder characteristics on the structural and the mechanical properties of additively manufactured Zr-based bulk metallic glass," *Materials and Design*, vol. 209, Article ID 109976, 2021.

[10] M. Ghidelli, A. Orekhov, A. L. Bassi et al., "Novel class of nanostructured metallic glass films with superior and tunable mechanical properties," *Acta Materialia*, vol. 213, Article ID 116955, 2021.

[11] M. Li, H. Guan, S. Yang, X. Ma, and Q. Li, "Minor Cr alloyed Fe–Co–Ni–P–B high entropy bulk metallic glass with excellent mechanical properties," *Materials Science and Engineering*, vol. 805, Article ID 140542, 2021.

[12] R. Sivaraman, I. Patra, Z. M. Najm, N. M. Hameed, T. Alawsi, and S. Hashemi, "The effects of minor element addition on the structural heterogeneity and mechanical properties of ZrCuAl bulk metallic glasses," *Advances in Materials Science and Engineering*, vol. 2022, Article ID 6528470, 8 pages, 2022.

[13] I. Patra, A. M. Abdulhadi, F. S. Fahim, B. S. Bashar, T. Alawsi, and M. Salmani, "The effects of temperature and impact velocity on the shock wave response of pore-embedded metallic glasses," *Advances in Materials Science and Engineering*, vol. 2022, Article ID 6111294, 8 pages, 2022.

[14] Z. Chen, Y. Xie, A. Datye et al., "Angstrom-scale replication of surfaces with crystallized bulk metallic glasses," *Materials Today Nano*, vol. 16, Article ID 100145, 2021.

[15] J. P. Singer, M. Gopinadhan, Z. Shao, A. D. Taylor, J. Schroers, and C. O. Osuji, "Nanoimprinting sub-100 nm features in a photovoltaic nanocomposite using durable bulk metallic glass molds," *ACS Applied Materials and Interfaces*, vol. 7, no. 6, pp. 3456–3461, 2015.

[16] X. Liang, P. Sharma, Y. Zhang, and H. Kato, "Nanoimprinting of magnetic FeCo-based metallic glass thin films," *Journal of Magnetism and Magnetic Materials*, vol. 542, Article ID 168455, 2022.

[17] L. Xiaoyu, P. Sharma, Y. Zhang, A. Makino, and H. Kato, "Nano-imprinting potential of magnetic FeCo-based metallic glass," *Nanotechnology*, vol. 30, Article ID 305302, 2019.

[18] M. Li, W. Luo, J. Xu, J. Zhang, K. W. Ng, and X. Cheng, "Fabrication and oxidation of amorphous Zr-based alloy for imprint lithography," *Microelectronic Engineering*, vol. 256, Article ID 111722, 2022.

[19] C. D. Wu and R. E. Li, "Effects of alloy composition, cavity aspect ratio, and temperature of imprinted ZrCu metallic glass films: a molecular dynamics study," *Applied Physics A*, vol. 126, no. 3, p. 209, 2020.

[20] D. Q. Doan, T. H. Fang, A. S. Tran, and T. H. Chen, "Residual stress and elastic recovery of imprinted Cu-Zr metallic glass films using molecular dynamic simulation," *Computational Materials Science*, vol. 170, Article ID 109162, 2019.

[21] C.-D. Wu and C.-J. Hou, "Molecular dynamics analysis of plastic deformation and mechanics of imprinted metallic glass films," *Computational Materials Science*, vol. 144, pp. 248–255, 2018.

[22] Y. Zhu, G. Liao, T. Shi, M. Li, Z. Tang, and F. Xiong, "Thermoplastic deformation and structural evolutions in nanoimprinting metallic glasses using molecular dynamics analysis," *Journal of Non-crystalline Solids*, vol. 427, pp. 46–53, 2015.

[23] J. P. Singer, C. I. Pelligra, N. Kornblum et al., "Multiscale patterning of a metallic glass using sacrificial imprint lithography," *Microsystems and Nanoengineering*, vol. 1, Article ID 15040, 2015.

[24] C. Wang, L. W. Nien, H. C. Ho, Y. C. Lai, and C. H. Hsueh, "Surface plasmon excited on imprintable thin-film metallic

glasses for surface-enhanced Raman scattering applications," *ACS Applied Nano Materials*, vol. 1, no. 2, pp. 908–914, 2018.

[25] C. D. Wu, "Atomistic simulation of nanoformed metallic glass," *Applied Surface Science*, vol. 343, pp. 153–159, 2015.

[26] A. S. Tran, D. Q. Doan, and V. T. Chu, "Molecular simulation study on mechanical properties and elastic recovery of nanoimprinted CuAgAu metallic glasses," *Journal of Non-crystalline Solids*, vol. 596, Article ID 121861, 2022.

[27] C. H. Wang, K. C. Chao, T. H. Fang, I. Stachiv, and S. F. Hsieh, "Investigations of the mechanical properties of nano-imprinted amorphous Ni–Zr alloys utilizing the molecular dynamics simulation," *Journal of Alloys and Compounds*, vol. 659, pp. 224–231, 2016.

[28] G. Kumar, J. Blawzdziewicz, and J. Schroers, "Controllable nanoimprinting of metallic glasses: effect of pressure and interfacial properties," *Nanotechnology*, vol. 24, no. 10, Article ID 105301, 2013.

[29] D. Lau, W. Jian, Z. Yu, and D. Hui, "Nano-engineering of construction materials using molecular dynamics simulations: prospects and challenges," *Composites Part B: Engineering*, vol. 143, pp. 282–291, 2018.

[30] D. Surblys, H. Matsubara, G. Kikugawa, and T. Ohara, "Application of atomic stress to compute heat flux via molecular dynamics for systems with many-body interactions," *Physical Review E*, vol. 99, no. 5, Article ID 51301, 2019.

[31] J. I. Odujole and S. Desai, "Molecular dynamics investigation of material deformation behavior of PMMA in nanoimprint lithography," *AIP Advances*, vol. 10, no. 9, Article ID 95102, 2020.

[32] H. W. Sheng, E. Ma, and M. J. Kramer, "Relating dynamic properties to atomic structure in metallic glasses," *Journal of Occupational Medicine*, vol. 64, no. 7, pp. 856–881, 2012.

[33] C. Braga and K. P. Travis, "A configurational temperature Nosé-Hoover thermostat," *The Journal of Chemical Physics*, vol. 123, no. 13, Article ID 134101, 2005.

[34] C. M. Meylan, F. Papparotto, S. Nachum et al., "Stimulation of shear-transformation zones in metallic glasses by cryogenic thermal cycling," *Journal of Non-crystalline Solids*, vol. 548, Article ID 120299, 2020.

[35] K. E. Avila, S. Küchemann, I. Alabd Alhafez, and H. M. Urbassek, "Shear-transformation zone activation during loading and unloading in nanoindentation of metallic glasses," *Materials*, vol. 12, no. 9, p. 1477, 2019.

[36] C. D. Wu, T. H. Fang, and J. F. Lin, "Effects of mold geometry and taper angles on the filling mechanism of a nanoimprinted polymer using molecular dynamics," *Applied Surface Science*, vol. 316, pp. 292–300, 2014.

[37] J. L. Gu, H. W. Luan, S. F. Zhao et al., "Unique energy-storage behavior related to structural heterogeneity in high-entropy metallic glass," *Materials Science and Engineering*, vol. 786, Article ID 139417, 2020.

[38] Y. Lou, X. Liu, X. Yang et al., "Fast rejuvenation in bulk metallic glass induced by ultrasonic vibration pre-compression," *Intermetallics*, vol. 118, Article ID 106687, 2020.